9th ECCOMAS Thematic Conference on the Mechanical Response of Composites
COMPOSITES 2023
G. Catalanotti, H. Petterman and G. Pittaresi (Eds)

MICROMECHANICAL HOMOGENIZATION METHODS OF A SHORT GLASS FIBRE-REINFORCED INJECTION-MOLDED BIO-BASED COMPOSITE MATERIAL

Oliver Schwahofer[a,*], Fermin Otero[b,c], Pedro Camanho [d,e] and Klaus Drechsler[a]

[a] Technical University of Munich, TUM School of Engineering and Design, Department of Aerospace and Geodesy, Chair of Carbon Composites
[b] CIMNE, Universitat Politècnica de Catalunya, 08034
[c] Department of Nautical Science and Engineering, Universitat Politècnica de Catalunya, 08003 Barcelona, Spain
[d]DEMec, Faculdade de Engenharia, Universidade do Porto, Porto, Portugal
[e] INEGI, Universidade do Porto, Porto, Portugal
[*] oliver.schwahofer@tum.de

Keywords: Modelling, Micromechanics, Short-fibre, composite, Elastic, Homogenization

Summary: *Herein, microscale approaches were explored to determine the homogenized properties of short fibre reinforced polymer material. The analytical homogenization follows the shear lag principle to approximate elastic modulus in the case of longitudinally oriented short fibres. For the finite element-based homogenization, a periodic 3D representative volume element of the composite is constructed to apply forward numerical homogenization. This unit cell is discretized by tetrahedral 3D finite elements resulting in a periodic mesh. An effective spring element method was further developed to homogenize the properties of short fibre-reinforced material. The reduced order spring method predicted the elastic properties almost equally to the finite element-based homogenization. A novel bio-based polyamide matrix with 40% glass fibre content and a traditional polyamide with 30% glass fibre reinforcement serve for the application and validation of the developed micromechanical methods. An additional effectivity parameter must be considered to capture the manufacturing imperfections of the injection molding process. This parameter can be calibrated based on experimental data from tensile testing. The developed numerical frameworks show good potential for extensions to more advanced modelling of the composite, such as nonlinear behaviour or failure mechanism.*

1 Introduction

Predicting the homogenized mechanical properties of short fibre-reinforced polymer (SFRP) is challenging. The reinforcing fibres' location, length and orientation may be random and hardly predictable. Additionally, manufacturing techniques for processing SFRP may suffer from imperfections which could also affect the mechanical performance

of the composite. All these aspects introduce an extra difficulty in estimating the mechanical properties compared to long fibre-reinforced polymers (LFRP). For instance, the principle of the well-known rule of mixture (RoM) cannot be directly applied, as short fibres receive the load from the matrix by shear, even in a perfectly longitudinal loading direction and longitudinally aligned fibre orientation. Due to this effect, the homogenized elastic properties depend on the distribution and the length of the fibres. The nonlinear mechanical behaviour and the failure mechanism are accordingly challenging to predict with traditional methods.
The target of the numerical homogenization methods is to reduce the time-consuming and complicated test amounts. SFRP was experimentally characterized in several works [1] [2] [3]. SFRP micromechanical homogenization is carried out in [4] and [5]. The forward finite element method (FEM) for the homogenized properties of 2D or 3D inhomogenous materials has an extensive literature. Along forward homogenization, a micromechanical representative volume element (RVE) is selected to model the smallest repeating unit of the material. This discretized RVE can be used to calculate the homogenized properties of the composite. FE-based elastic homogenization was explored by [6] [3] [7] [8] [9]. Various micromechanical nonlinear homogenization methods were explored in [10] [3] [11] [12] [2] [13] to model the nonlinear behaviour of the composite.
In this paper, the elastic properties of a glass fibre-reinforced traditional polyamide (PA) material and a novel bio-based PA material are analyzed. The traditional composite has a fibre volume of 30 %, while the bio-based alternative has 40 % glass fibre content. The stress-strain relationship of the pure glass fibre, pure bio-based thermoplastic, pure traditional thermoplastic are plotted in Figure 1. The stress-strain curves are derived from standard quasistatic tensile tests. The novel bio-based PA has around 30 % lower elasticity (E_m) than the traditional PA. The elasticity of the glass fibre (E_f) is 70 GPa.

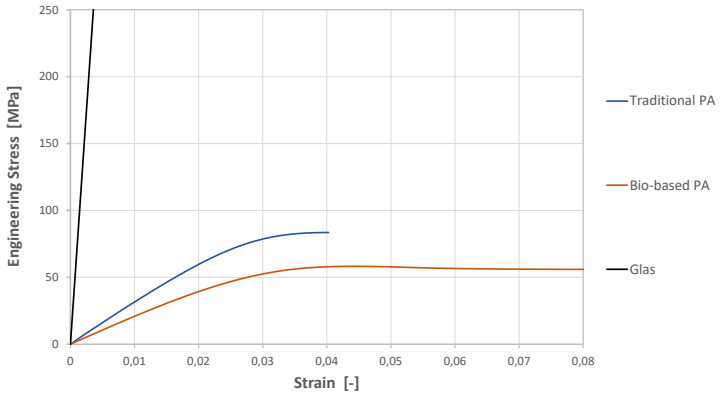

Figure 1: Stress-strain relationship under tensile testing of the pure matrices and fibre material

Analytical and numerical homogenization techniques will be revealed in order approximate the mechanical properties of the bio-based and traditional SFRPs. The main target of this research to find an effective method to understand the material behaviour. This gives the chance to optimize the novel bio-based composite, and therefore help its industrialization.

2 Analytical homogenization

For short fibre reinforcement, the shear lag [14] approach can be used to analytically estimate the elasticity of the material considering longitudinal fibre orientations. The method is based on the load transfer mechanism in discontinuous fibres. The theory introduces a critical length (l_c). Below this length, the reinforcing fibres do not contribute with their total loading capacity. Figure 2 demonstrates the shear and normal stress distribution of a single discontinuous fibre. An RVE of a single short fibre and its surrounding matrix is taken to derive the homogenized elastic properties of the composite as it is seen in Figure 2. The outer diameter of the single-fibre RVE is chosen to meet the prescribed fibre-volume fraction (ϕ). This can be modified based on Tucker [15] by applying Cox, Hexagonal or Square packing.

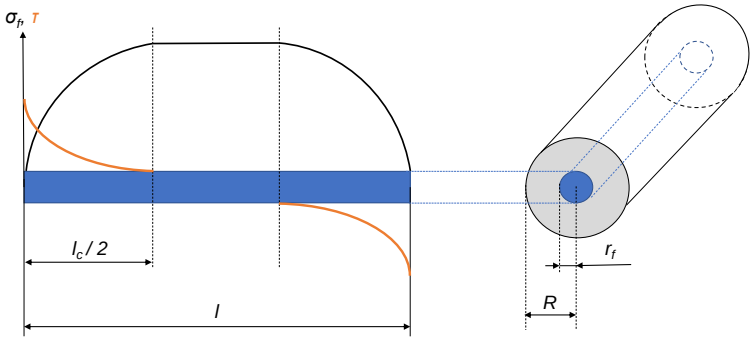

Figure 2: Single fibre normal stress and shear stress distribution

Based on the shear stress distribution of the single-fibre RVE, [14] derives eq. 1 for the longitudinal Young's Modulus of purely longitudinally oriented short fibres. In eq. 1, E_f and E_m indicate the elastic modulus of the fibre and the matrix materials, while l stands for the fibre length.

$$E_0 = E_f * \phi * \left(1 - \frac{tanh(\frac{\beta l}{2})}{\frac{\beta l}{2}}\right) + E_m * (1 - \phi), \tag{1}$$

where β depends on the RVE geometry (Figure 2) and shear modulus of the matrix (G_m):

$$\beta^2 = \frac{G_m}{E_f}\left(\frac{2\pi}{A_f * ln(r_f/R)}\right). \tag{2}$$

Hypothetically, some of the short fibres may not be perfectly bonded with the matrix, which results in the ineffectiveness of some fibres within the composite volume. To model this effect, the longitudinal elasticity formula in eq. 1 was modified with an additional parameter (p_{eff}) to model the ineffective fibres. This parameter can be then calibrated based on experimentally characterized data.

$$E_{00,eff} = E_f * p_{eff} * \phi * \left(1 - \frac{tanh(\frac{\beta l}{2})}{\frac{\beta l}{2}}\right) + E_m * (1 - \phi) \tag{3}$$

To homogenize the varying short fibre lengths, a weighted average formulation was established in eq. 4. N represents the total number of recognizable fibre lengths, while n_i corresponds to the occurrence of the given fibre length within the composite. The fibre lengths and their occurrence can be determined from computer tomography (CT) scans of the tested specimen. The exact experimental setup and CT scan images are not detailed in this work.

$$E_0 = \sum_{i=1}^{N} \frac{n_i * E_{00,i}}{N} \tag{4}$$

With the formulation from eq. 4, the reduced longitudinal elasticity can be captured. Nevertheless, direct comparison with the experimentally characterized Young's Modulus is only possible if the varying orientation of the fibres in the manufactured specimen is considered. CT scan images can typically record the fibre orientation tensor (A_{ii}) of a test specimen. This diagonal tensor indicates the probability of the fibre orientations in the three rectangular coordinate directions. The effect of the varying fibre orientations is not further analyzed in this work.

3 Numerical homogenization

Beyond the presented analytical method in section 2, FEM and the reduced order spring element method (SEM) were implemented to virtually characterize the homogenized properties of SFRP. Both methods works with a numerically discretized RVE that models several randomly distributed fibres in transverse and longitudinal directions. While in the analytical approach, only a single-fibre RVE was considering perfect packing.

3.1 Finite Element Method (FEM)

A Python tool was developed that can generate a 3D short-fibre RVE geometry in the form of a cuboid. The unit cell dimension, the fibre length and diameter, and the fibre volume fraction can be selected as parameters. The tool assigns random locations of the fibres avoiding collisions between them, meanwhile fulfilling 3D periodicity. Fibres are positioned aligned, but rotation around an arbitrary vector is possible. Linear tetrahedral finite elements are used for the discretization which is carried out through a Python-Gmsh tool. A thin 3D-meshed interface layer between the fibres and matrix is optional, but inactivated for the linear elastic homogenizations. Calculations are carried out in Abaqus software, applying periodic boundary conditions and prescribed strains in the six principal directions [16]. The RVE tool is summarized in Figure 3.

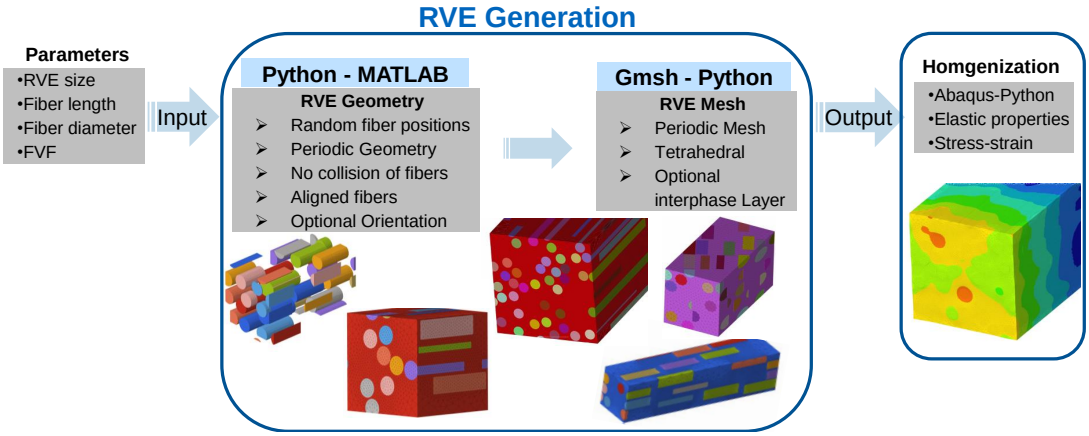

Figure 3: Homogenization tool using FE-meshed micro RVE

Convergence studies were carried out to find the ideal mesh size and RVE dimensions. For the analysis of RVEs with perfectly longitudinally aligned fibres, the transversal dimensions of the cuboid are selected as 4 times the fibre diameter. In the longitudinal direction, the RVE should be around 2.5 times larger than the fibre length to achieve convergence. Depending on the geometric setup of the composite, such an RVE requires about 30.000 nodes for the FE discretization. The number of degrees of freedom even increases rapidly, in case a 3D interphase layer is desired (e.g. for nonlinear elastoplastic simulation).

3.2 Spring Element Method (SEM)

A spring element method is presented to predict the homogenized properties of perfectly longitudanally oriented short fibre composite material. SEM was first proposed by Okabe et al. [17] as a reduced order alternative compared to FEM. Tavares et al. [18] implemented the Spring element method to model the failure of LFRP considering random fibre distribution. This framework was further developed to adjust the capabilities for modelling short fibre-reinforced materials.

Tavares et al. [18] tackled only high-fibre content, high-fibre elasticity composites, the longitudinal matrix contribution was neglected, and the matrix only contributed to the stiffness in the form of transversal shear springs. To model the contribution of the matrix to the longitudinal elastic modulus of the composite, a new formulation is proposed in this work. Between the longitudinal fibre elements, longitudinal matrix spring elements are introduced. For that reason, the linear transversal shear springs were upgraded to quadratic springs to add the new longitudinal matrix springs to the system. So, the new approach considers linear longitudinal spring element (SE) for the fibres and matrix and quadratic lateral SE for the matrix.

A micro connectivity system between two longitudinal fibre segments and one connecting matrix shear springs are shown in Figure 4. The newly formed quadratic spring element and interconnecting longitudinal element are marked with orange colour.

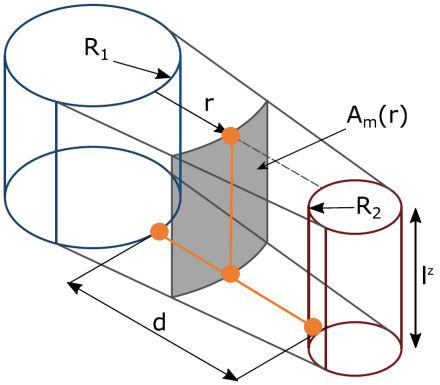

Figure 4: The new quadratic SE formulation

The effective area of the shear matrix element is expressed as

$$A_m(r) = A_m^1 + \frac{(A_m^2 - A_m^1)}{d} r, \tag{5}$$

where

$$A_m^1 = \frac{2\pi R_1}{n_1} l^z \quad ; \quad A_m^2 = \frac{2\pi R_2}{n_1} l^z. \tag{6}$$

The stiffness matrix of the finite element for the matrix is obtained as

$$K_m = \int_0^d B^T(r) G A_m(r) B(r)\ dr, \tag{7}$$

where

$$B(r) = \frac{\partial N(r)}{\partial r}, \tag{8}$$

where N indicates the shape vector functions.
In the case of a quadratic finite element, the shape functions are:

$$N(r) = [N_1(r)\ , N_2(r)\ , N_3(r)] = \left[1 - \frac{3r}{d} + \frac{2r^2}{d^2},\ \frac{4r}{d} - \frac{4r^2}{d^2},\ -\frac{r}{d} + \frac{2r^2}{d^2}\right]. \tag{9}$$

With quadratic shape functions, the stiffness matrix for the shearing SE yields

$$K_m^s = \frac{G}{d^2} \int_0^d \begin{bmatrix} 9 - \frac{24r}{d} + \frac{16r^2}{d^2} & -12 + \frac{40r}{d} - \frac{32r^2}{d^2} & 3 - \frac{16r}{d} + \frac{16r^2}{d^2} \\ & 16 - \frac{64r}{d} + \frac{64r^2}{d^2} & -4 + \frac{24r}{d} - \frac{32r^2}{d^2} \\ Sym & & 1 - \frac{8r}{d} + \frac{16r^2}{d^2} \end{bmatrix} A_m(r)\ dr. \tag{10}$$

After plugging in $A_m(r) = A_m^1 - A_m^1 \frac{r}{d} + A_m^2 \frac{r}{d}$ into eq. 10, it is possible to find the stiffness matrix as:

$$K_m^s = \frac{G}{d} \begin{bmatrix} \frac{1}{2}A_m^2 + \frac{11}{6}A_m^1 & -\frac{2}{3}A_m^2 - 2A_m^1 & \frac{1}{6}A_m^2 + \frac{1}{6}A_m^1 \\ & \frac{8}{3}A_m^2 + \frac{8}{3}A_m^1 & -2A_m^2 - \frac{2}{3}A_m^1 \\ Sym & & \frac{11}{6}A_m^2 + \frac{1}{2}A_m^1 \end{bmatrix}. \tag{11}$$

The new linear longitudinal interconnecting matrix element formulation corresponds to the stiffness matrix of the longitudinal fibre elements from [18]. To model short fibre materials, some longitudinal fibre segments are assigned to matrix elements. The random distribution is realized with a constant longitudinal matrix segment length formulation. In this sense, the SEM is more restricted to the FEM approach, where the longitudinal fibre gaps are also randomly distributed.

4 Results and Discussion

4.1 Analytical distributions

The fibre length dependency on the longitudinal elastic modulus (E_0 from equation eq. 1) by the shear lag model is shown in Figure 5. The distributions consider the fibre volume content ($\phi_1 = 0.3$ and $\phi_2 = 0.4$) and matrix elasticity ($E_{m,1} = 3100$ and $E_{m,2} = 2100$ MPa) according to the traditional and the new bio-based composites. Figure 5 also plots the homogenized transverse elasticity (E_{90}) through the inverse rule of mixture (iRom) that is usually valid for LFRPs. A constant fibre diameter ($d_f = 0.0012$ mm) is considered.

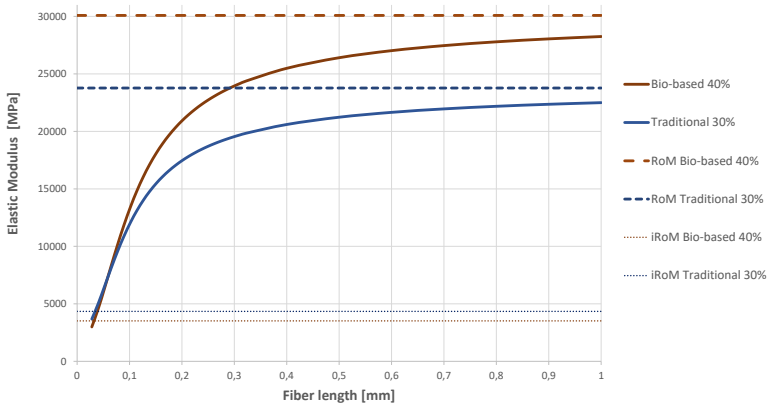

Figure 5: The longitudinal elasticity over the short fibre lengths

Figure 5 indicates the high drop of in the stiffness as the fibre length decreases. The analytical distributions suggest that the traditional composite is slightly stiffer in the case of very short fibre lengths. The aspect ratio (d_f/l_f) of the short fibre is close to 1, and the longitudinal elasticity is near the transversal modulus. That results in a quasi-isotropic configuration, where the stiffer traditional PA ($E_{m,1}$) contributes more to the homogenized elasticity. As the aspect ratio rises, the bio-based composite ($\phi_2 = 0.4$) becomes more and more stiffer. That means that the higher fibre content compensates for the lower elasticity of the bio-based PA ($E_{m,2}$), as the reinforcing fibres are more and more loaded through their increasing lengths. At very high aspect ratio regions, the homogenized stiffness approaches the elasticity from the RoM, which is applied regularly on LFRP materials.
In the contrary, based on experimental data, the traditional composite outperforms the bio-based one in terms of stiffness. This already indicates that further modelling considerations must be applied to estimate the actual elastic properties of the composite. The derived weighted average eq. 4 of the composites are considerable softer, as expected from the experimental characterization. Direct comparison with the experimental results is not

possible as the analytical formulation considers perfectly longitudinal fibre orientations, which is never exactly achieved in reality.
The fibre length weighted average elasticity from eq. 4 overestimates the expected longitudinal elastic modulus with 30-35 % for the traditional composite, and with 45-50 % the bio-based material. The reasons for this deviation must be explained with manufacturing imperfections.
Based on the testing data of the traditional and bio-based material, the manufacturing-related p_{eff} from equation eq. 3 was calibrated. The elasticity of the traditional composite can be captured with $p_{eff} = 0.65$. At the same time, the bio-based material with higher fibre volume fraction can be modelled with considerably lower $p_{eff} = 0.38$. That means that due to the higher fibre volume, more fibres are ineffective in the material, which brings a contra-productive effect on the material's mechanical performance. For the calibration of p_{eff}, CT scan-based fibre length and fibre orientation distributions were also considered, but this is not detailed in this work.

4.2 Numerical RVE Homogenizations

In this work, only RVEs with constant fibre length were analyzed. Therefore, the same results can be generated through FE homogenization as through the analytical formulation in section 4.1, considering perfectly aligned orientation and varying lengths of the fibres. The analytical distributions were plotted in Figure 5, and they are used to compare with the FE-based prediction.

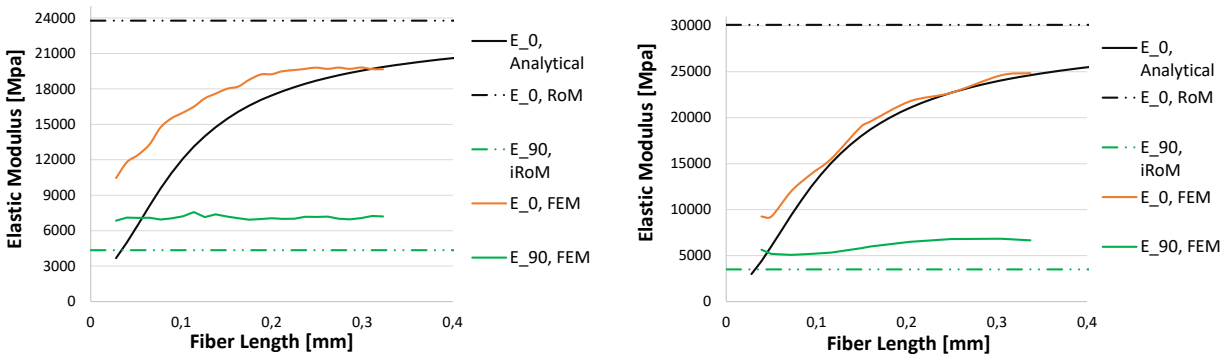

(a) Traditional composite ($\phi = 0.3$) (b) Bio-based composite ($\phi = 0.4$)

Figure 6: Analytical and FE-based Homogenization of longitudinal elasticity

Firstly, Figure 6 (a) shows the distributions for the traditional composite. The FE-based homogenization shows an acceptable agreement with the analytical approach for longer fibres ($0.2 - 0.3$ mm). However, it strongly overestimates the analytically derived elastic modulus at the low fibre length range.

The reason for that can be explained by the random location of the fibres in the FE unit cell. Some RVEs may have larger distance between fibres, while others could have some regions where some fibres are almost touching each other. The latter case

introduces an extra local reinforcement effect that makes the estimate considerably stiffer than the analytical formula. After some repeated executions of short-length fibre RVEs, this hypothesis was confirmed. Two exemplary RVEs demonstrate this effect in figure 7.

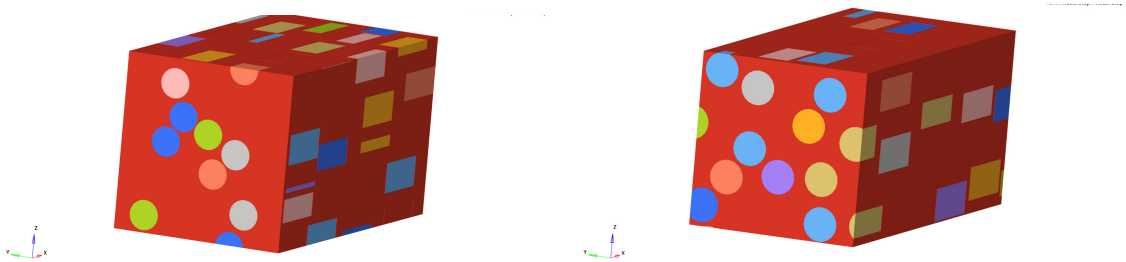

(a) $E_0 = 10.600$ MPa (b) $E_0 = 7600$ MPa

Figure 7: FE-meshed RVEs with small fibre distance zones (a) and larger gaps (b)

After introducing a minimum fibre distance constraint to the RVE tool, the FE homogenizations delivered lower homogenized elastic properties at the very short fibre length range.This effect can barely be observed in the bio-based material analysis, as the FE calculations follow the analytical distribution in Figure 6 (b) very well.

Due to the higher fibre volume fraction of bio-based configuration, the fibres are way more tightly packed within the RVE. Consequently, the above discussed randomly occurring "local reinforcement" by tiny gaps is less likely to happen.

The SEM was also tested on the configuration of the traditional composite. Simulations were carried out with varying matrix length choices. The longitudinal gaps between the fibres slightly affected the homogenized elastic property. The longitudinal matrix segment lengths (l_m) were tested as $l_m = l_f$, $l_m = 0.5 * l_f$ and $l_m = 0.25 * l_f$. Figure 8 plots the FE-homogenized and SE-homogenized longitudinal elastic properties of the traditional composite ($\phi = 0.3$).

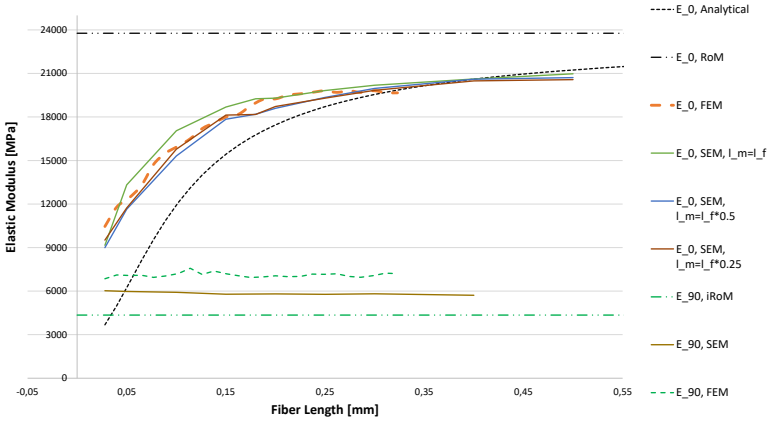

Figure 8: Comparison between FEM and SEM with varying matrix segment lengths using the traditional composite configuration

A 2D mesh of one slice of the SE-RVE applying the new quadratic formulation can be seen in Figure 9 a), where the system of longitudinal fibre elements (full green), longitudinal matrix elements (black circle) and shear matrix elements (red line) can be captured. After the extrusion of a single 2D slice in the third direction, the full RVE is built. Figure 9 b) shows the RVE through longitudinal expansion. The red segments represent the longitudinal matrix, while the blue springs indicate the reinforcing glass fibre elements.

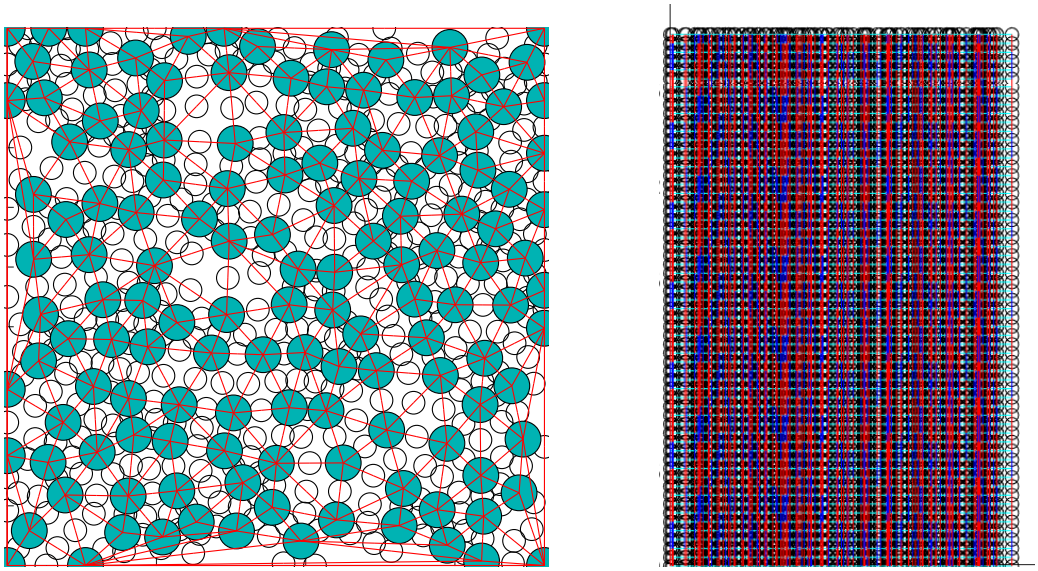

(a) 2D slice of RVE (b) Expansion in longitudinal direction

Figure 9: SE-meshed RVE

5 Conclusion

In this work, analytical and numerical micromechanical methods were presented to estimate the homogenized mechanical properties of two SFRP materials. The fibre length-dependent behaviour of the SFRP is captured well through all methods (analytical formulation, FEM and SEM). Manufacturing imperfections must be considered in order to obtain realistic homogenized properties. Hence the effectivity parameter (p_{eff}) was introduced that can be calibrated for elastic homogenizations based on experimental data. The analytical model and the SEM work well for elasticity but they have limitations in modelling rotated fibre orientations. Varying fibre orientation can be modelled with FEM, furthermore, extension to nonlinear elastoplastic homogenization is possible through 3D-discretized cohesive zones. However, the computational effort of FE calculations increases rapidly as more complex analyses are targeted. For that reason, the enhancement of the SEM to a nonlinear solver shows great potential to reduce computational costs in predicting the nonlinear stress-strain behaviour or failure simulation of SFRP materials. The nonlinear SE homogenization approach already delivered very good results for quasistatic [18] and dynamic [19] LFRP applications.
The presented homogenization methods help to improve the mechanical performance of the novel bio-based composite. This innovative material can then replace conventional SFRPs in industrial structural components using injection molding manufacturing.

Acknowledgments and Compliance with Ethical Standards

This work was supported by the Federal Ministry for Economic Affairs and Climate Action of Germany in the frame of the public research project 'COOPERATE'. The authors express their gratitude contribution to the project partners: BOGE Elastmetall GmbH, TECNARO GmbH and Fraunhofer Institute LBF.
The authors declare that they have no conflict of interest.

REFERENCES

[1] Li, Y., Pimenta, S., Singgih, J., Nothdurfter, S., Schuffenhauer, K.: Experimental investigation of randomly-oriented tow-based discontinuous composites and their equivalent laminates. Composites Part A: Applied Science and Manufacturing **102**, 64–75 (2017). https://doi.org/10.1016/j.compositesa.2017.06.031

[2] Alves, M., Martulli, L.M., Kerschbaum, M., Swolfs, Y., Lomov, S.V., Pimenta, S. (eds.): A 3D Finite Element Stochastic Framework for the Failure of Tow-based Discontinuous Composites, vol. 232 (2023). https://doi.org/10.1016/j.compscitech.2022.109846

[3] Mirkhalaf, S.M., Eggels, E.H., van Beurden, T.J.H., Larsson, F., Fagerström, M.: A finite element based orientation averaging method for predicting elastic properties of short fiber reinforced composites. Composites Part B: Engineering **202**, 108388 (2020). https://doi.org/10.1016/j.compositesb.2020.108388

[4] Doghri, I., Tinel, L.: Micromechanical modeling and computation of elasto-plastic materials reinforced with distributed-orientation fibers. International Journal of Plasticity **21**(10), 1919–1940 (2005). https://doi.org/10.1016/j.ijplas.2004.09.003

[5] Henry, J., Pimenta, S. (eds.): Semi-analytical Simulation of Aligned Discontinuous Composites, vol. 144 (2017). https://doi.org/10.1016/j.compscitech.2017.01.027

[6] Naili, C., Doghri, I., Kanit, T., Sukiman, M.S., Aissa-Berraies, A., Imad, A.: Short fiber reinforced composites: Unbiased full-field evaluation of various homogenization methods in elasticity. Composites Science and Technology **187**, 107942 (2020). https://doi.org/10.1016/j.compscitech.2019.107942

[7] El Moumen, A., Kanit, T., Imad, A.: Numerical evaluation of the representative volume element for random composites. European Journal of Mechanics - A/Solids **86**, 104181 (2021). https://doi.org/10.1016/j.euromechsol.2020.104181

[8] D'Mello, R.J., Waas, A.M.: Influence of unit cell size and fiber packing on the transverse tensile response of fiber reinforced composites. Materials (Basel, Switzerland) **12**(16) (2019). https://doi.org/10.3390/ma12162565

[9] Zhong, Y., Liu, P., Pei, Q., Sorkin, V., Louis Commillus, A., Su, Z., Guo, T., Thitsartarn, W., Lin, T., He, C., Zhang, Y.-W.: Elastic properties of injection molded short

glass fiber reinforced thermoplastic composites. Composite Structures **254**, 112850 (2020). https://doi.org/10.1016/j.compstruct.2020.112850

[10] Savvas, D., Stefanou, G., Papadrakakis, M.: Determination of rve size for random composites with local volume fraction variation. Computer Methods in Applied Mechanics and Engineering **305**, 340–358 (2016). https://doi.org/10.1016/j.cma.2016.03.002

[11] Islam, M., Tudryn, G.J., Picu, C.R.: Microstructure modeling of random composites with cylindrical inclusions having high volume fraction and broad aspect ratio distribution. Computational Materials Science **125**, 309–318 (2016). https://doi.org/10.1016/j.commatsci.2016.08.051

[12] Ahmadi, H., Hajikazemi, M., van Paepegem, W.: Predicting the elasto-plastic response of short fiber reinforced composites using a computationally efficient multiscale framework based on physical matrix properties. Composites Part B: Engineering **250**, 110408 (2023). https://doi.org/10.1016/j.compositesb.2022.110408

[13] Wang, L., Nygren, G., Karkkainen, R.L., Yang, Q.: A multiscale approach for virtual testing of highly aligned short carbon fiber composites. Composite Structures **230**, 111462 (2019). https://doi.org/10.1016/j.compstruct.2019.111462

[14] Ayal de S. Jayatilaka (ed.): Fracture of Engineering Brittle Materials. Applied Science Publisher, London (1979)

[15] Tucker, C., L.: Stiffness predictions for unidirectional short-fiber composites_ review and evaluation. Comosite Science and Technology (1998)

[16] Omairey, S.L., Dunning, P.D., Sriramula, S.: Development of an abaqus plugin tool for periodic rve homogenisation. Engineering with Computers **35**(2), 567–577 (2019). https://doi.org/10.1007/s00366-018-0616-4

[17] Okabe, T., Sekine, H., Ishii, K., Nishikawa, M., Takeda, N.: Numerical method for failure simulation of unidirectional fiber-reinforced composites with spring element model. Composites Science and Technology **65**(6), 921–933 (2005). https://doi.org/10.1016/j.compscitech.2004.10.030

[18] Tavares, R.P., Otero, F., Turon, A., Camanho, P.P.: Effective simulation of the mechanics of longitudinal tensile failure of unidirectional polymer composites. International Journal of Fracture **208**(1-2), 269–285 (2017). https://doi.org/10.1007/s10704-017-0252-9

[19] Tavares, R.P., Otero, F., Baiges, J., Turon, A., Camanho, P.P.: A dynamic spring element model for the prediction of longitudinal failure of polymer composites. Computational Materials Science **160**, 42–52 (2019). https://doi.org/10.1016/j.commatsci.2018.12.048